Molecular Biology of the Cell
Vol. 17, 4801–4811, November 2006

Caenorhabditis elegans DYF-2, an Orthologue of Human WDR19, Is a Component of the Intraflagellar Transport Machinery in Sensory Cilia[V]

Evgeni Efimenko,* Oliver E. Blacque,† Guangshuo Ou,‡ Courtney J. Haycraft,§ Bradley K. Yoder,§ Jonathan M. Scholey,‡ Michel R. Leroux,† and Peter Swoboda*

*Karolinska Institute, Department of Biosciences and Nutrition, Södertörn University College, School of Life Sciences, S-14189 Huddinge, Sweden; †Department of Molecular Biology and Biochemistry, Simon Fraser University, Burnaby, British Columbia, V5A 1S6 Canada; ‡Center for Genetics and Development, Section of Molecular and Cellular Biology, University of California, Davis, Davis, CA 95616; and §Department of Cell Biology, University of Alabama at Birmingham Medical Center, Birmingham, AL 35294

Submitted April 3, 2006; Revised August 14, 2006; Accepted August 22, 2006
Monitoring Editor: Erika Holzbaur

The intraflagellar transport (IFT) machinery required to build functional cilia consists of a multisubunit complex whose molecular composition, organization, and function are poorly understood. Here, we describe a novel tryptophan-aspartic acid (WD) repeat (WDR) containing IFT protein from *Caenorhabditis elegans*, DYF-2, that plays a critical role in maintaining the structural and functional integrity of the IFT machinery. We determined the identity of the *dyf-2* gene by transgenic rescue of mutant phenotypes and by sequencing of mutant alleles. Loss of DYF-2 function selectively affects the assembly and motility of different IFT components and leads to defects in cilia structure and chemosensation in the nematode. Based on these observations, and the analysis of DYF-2 movement in a Bardet–Biedl syndrome mutant with partially disrupted IFT particles, we conclude that DYF-2 can associate with IFT particle complex B. At the same time, mutations in *dyf-2* can interfere with the function of complex A components, suggesting an important role of this protein in the assembly of the IFT particle as a whole. Importantly, the mouse orthologue of DYF-2, WDR19, also localizes to cilia, pointing to an important evolutionarily conserved role for this WDR protein in cilia development and function.

INTRODUCTION

Cilia and flagella are subcellular organelles exposed from the cell surface. They are highly conserved in evolution and play important roles in cell motility, sensory stimuli reception, and early developmental processes. In humans cilia are almost ubiquitously present on many different cell types. Defects in their structure or function lead to a wide range of developmental problems and diseases (Pazour and Rosenbaum, 2002; Rosenbaum and Witman, 2002; Scholey, 2003; Afzelius, 2004).

The general architecture of cilia and their close relatives, flagella, consists of a microtubule-based axonemal core enclosed by a membrane (Perkins *et al*., 1986; Dutcher, 1995). The assembly and further structural and functional maintenance of cilia and flagella are dependent on the process of intraflagellar transport (IFT). During IFT, nonmembrane-bound particles (IFT particles) and their associated cargo molecules are moved continuously along the axoneme by means of kinesin-2 and IFT-dynein molecular motors that mediate their anterograde and retrograde transport, respectively (Kozminski *et al*., 1993; Cole *et al*., 1993; Kozminski *et al*., 1995; Morris and Scholey, 1997; Pazour *et al*., 1999; Porter *et al*., 1999; Signor *et al*., 1999a,b; Schafer *et al*., 2003; Lawrence *et al*., 2004; Snow *et al*., 2004).

Significant information about the biological properties of IFT particles was obtained from the studies of motile flagella in the green alga *Chlamydomonas reinhardtii* and of sensory cilia in the nematode *Caenorhabditis elegans*. It has been shown that IFT particles in *Chlamydomonas* consist of 16 or more proteins (Piperno and Mead, 1997), which can biochemically be resolved into two complexes: A and B (Cole *et al*., 1998; Piperno *et al*., 1998). In *C. elegans*, IFT-A and IFT-B proteins fall into two different complexes based on ciliary phenotypes in mutant worms. Thus, mutants of complex B (CHE-2, CHE-13, DYF-3, OSM-1, OSM-5, OSM-6) typically show a drastic reduction of cilia length (Cole *et al*., 1998; Collet *et al*., 1998; Fujiwara *et al*., 1999; Signor *et al*., 1999b; Haycraft *et al*., 2001; Haycraft *et al*., 2003; Murayama *et al*., 2005; Ou *et al*., 2005b). In contrast, mutants of complex A (CHE-11 or DAF-10) have only slightly reduced cilia with massive accumulation of IFT particles along the axoneme (Qin *et al*., 2001). These data suggested that complex B proteins are necessary for anterograde directed movement of IFT particles, whereas complex A components function in retrograde transport (Perkins *et al*., 1986; Qin *et al*., 2001; Haycraft *et al*., 2003; Schafer *et al*., 2003).

According to a recent model IFT is a complex, multistep process that includes the following events: assembly of motors, IFT particles, and cargo molecules in the basal body region; anterograde transport of IFT complex A and B and

This article was published online ahead of print in *MBC in Press* (http://www.molbiolcell.org/cgi/doi/10.1091/mbc.E06–04–0260) on September 7, 2006.

[V] The online version of this article contains supplemental material at *MBC Online* (http://www.molbiolcell.org).

Address correspondence to: Peter Swoboda (peter.swoboda@biosci.ki.se).

cargo such as inactive dynein by kinesin-2; release; dissociation and subsequent reassociation of the IFT particle; kinesin-2 and dynein molecules at the ciliary tip (the IFT particle binds to active dynein via complex A, whereas kinesin-2 binds to active dynein independently of complexes A or B); and retrograde transport of all components by active dynein and recycling of IFT components to the cell body (Pedersen *et al*., 2006).

Sensory cilia in *C. elegans* have a compartmentalized structure, consisting of a transition zone and a middle and a distal segment (Perkins *et al*., 1986; Snow *et al*., 2004). It has been shown that *C. elegans* Bardet–Biedl syndrome (BBS) proteins play selective roles in the assembly of IFT particle components at the base of cilia (Blacque *et al*., 2004). In *bbs-7* and *bbs-8* mutants, IFT-A and IFT-B particles can be driven separately along the middle and distal segments of the cilium by means of two distinct kinesin-2 motor complexes, kinesin-II and OSM-3-kinesin, respectively (Ou *et al*., 2005a). Thus, the transport of IFT-particles and BBS proteins along sensory cilia depends on the cooperation of kinesin-II and OSM-3-kinesins that form different ciliary segments by two sequential IFT-pathways: a middle segment pathway driven by kinesin-II and OSM-3 together and a distal segment pathway driven by OSM-3 alone (Snow *et al*., 2004; Ou *et al*., 2005a; Evans *et al*., 2006).

To improve our understanding of the IFT machinery, we are identifying the full repertoire of molecules involved in this process. For this purpose, we use *C. elegans*, where various genetic screens for sensory cilia mutants generated a large number of candidate genes. Depending on mutant phenotypes, these genes can be subdivided into one or more of the following classes: *osm*otic avoidance defective (osm), *che*motaxis and *od*orant *r*esponse defective (*che* and *odr*), *da*uer *f*ormation defective (*daf*), and fluorescent *dye*-filling defective (*dyf*) (Culotti and Russell, 1978; Bargmann *et al*., 1993; Malone and Thomas, 1994; Starich *et al*., 1995). Mutations that reduce fluorescent dye filling of the amphid and phasmid ciliated sensory neurons, which are directly exposed to the environment, are indicative of general defects in cilium structure and are often accompanied by other sensory mutant phenotypes (Starich *et al*., 1995). So far, mutations in most identified IFT genes result in a Dyf phenotype. Therefore, we concentrated our efforts on this class of ciliary mutants, which is comprised of 13 members, *dyf-1* to *dyf-13*.

In *C. elegans*, the expression of many ciliary genes is regulated by DAF-19, an RFX-type transcription factor that recognizes DNA sequence motifs (X-boxes) in promoters of its target genes (Swoboda *et al*., 2000; Fan *et al*., 2004; Efimenko *et al*., 2005; Blacque *et al*., 2005). Recently, three *dyf* genes (*dyf-1*, *dyf-3* and *dyf-13*) were cloned and their importance for the development of cilia has been demonstrated (Blacque *et al*., 2005; Murayama *et al*., 2005; Ou *et al*., 2005a,b). In all three cases, knowledge of the X-box sequence motif was crucial for the determination of gene identity.

In our current work, we describe another member of this class, the gene *dyf-2*, which is orthologous to human *WDR19*. Using the X-box promoter motif as a search tool for ciliary genes, we were able to easily clone *dyf-2*. We defined its structure and characterized available mutant alleles. We observed severe defects in cilia of *dyf-2* mutant worms, which is consistent with a ciliogenic role of *dyf-2*. Similar to many other *C. elegans* genes involved in cilia formation, *dyf-2* expression requires the proper function of DAF-19. Using different genetic and cell biological approaches we have shown that DYF-2 is a novel component that can associate with IFT particle complex B. At the same time, DYF-2 interferes with the function of complex A components, suggesting an intermediate nature of this protein within the IFT complex. We demonstrated that the expression of WDR19 is also related to ciliary structures in mammals. Given the very high sequence conservation between DYF-2 and WDR19, the study of DYF-2 in *C. elegans* will uncover WDR19 functions in humans.

MATERIALS AND METHODS

Worm Strains

Growth and culture of *C. elegans* strains were carried out following standard procedures (Brenner, 1974). The following strains were used for this study: wild-type N2 Bristol; CB1033 *che-2*(*e1033*); CB3323 *che-13(e1805)*; DR1120 *dyf-2(m543)*; JT204 *daf-12(sa204)*; JT6924 *daf-19(m86); daf-12(sa204)*; KD8802 *dyf-2*(*m160*); *mnIs17*[*osm-6::gfp*; *unc-36*(+)]; MX322 *bbs-8*(*nx77*); *nxEx*[*dyf-2::gfp*]; OE3050 *dyf-2*(*m160*); *ofEx38*[*dyf-2::gfp*; *rol-6*(*su1006*)]; OE3069 *che-11*(*e1810*); *ofEx46*[*dyf-2::gfp*; *rol-6*(*su1006*)]; OE3074 *che-13*(*e1805*); *ofEx47*[*dyf-2::gfp*; *rol-6*(*su1006*)]; OE3095 *dyf-2*(*m160*); *ofEx67*[*bbs-7::gfp*; *rol-6*(*su1006*)]; OE3244 *dyf-2*(*m160*); *ofEx193*[*dyf-2::gfp*; *myo-2::rfp*]; PT50 *che-11*(*e1810*); *myEx10*[*che-11::gfp*; *rol-6*(*su1006*)]; SP1234 *dyf-2(m160)*; YH20 *osm-5*(*p813*); *yhEx20* [*osm-5::gfp*; *rol-6*(*su1006*)]; YH101 *dyf-2*(*m160*); *yhEx19*[*osm-5::gfp*; *rol-6*(*su1006*)]; YH109 *dyf-2*(*m160*); *yhEx69*[*che-13::yfp*; *rol-6*(*su1006*)]; YH130 *che-13*(*e1805*); *yhEx90*[*che-13::gfp*; *rol-6*(*su1006*)]; YH397 *dyf-2*(*m160*); *myEx10*[*che-11::gfp*; *rol-6*(*su1006*)]. All strains used and strain construction details are available on request.

Molecular Characterization of the dyf-2 Gene

About 12-kb of genomic region, covering both the ZK520.3 and ZK520.1 predicted open reading frames (ORFs) were amplified from *dyf-2(m160)* and *dyf-2(m543)* worms, subcloned in smaller fragments and sequenced to identify possible mutations. The *dyf-2* cDNA was amplified from a wild-type N2 cDNA library (Haycraft *et al*., 2003), analyzed by sequencing, and used for functional tests as described below. Protein domain analysis was performed with the help of SMART (http://smart.embl-heidelberg.de) and Pfam (http://www.sanger.ac.uk/Software/Pfam) databases.

Dye-filling and Behavioral Assays

Fluorescent dye-filling assays were performed as described previously (Starich *et al*., 1995) by using the fluorescent dye DiI. Stained adult hermaphrodites were analyzed at 1000× magnification by conventional fluorescence microscopy (Axioplan 2; Carl Zeiss AG, Göttingen, Germany). The fluorescent dye-filling defective worm strain CB3323 was used as a control for the Dyf phenotype. Osmotic avoidance assays were performed essentially as described previously (Culotti and Russell, 1978) by testing the ability of adult hermaphrodite worms to cross a ring of high osmotic strength (8 M glycerol). All tests were done during a time period of 10 min. The osmotic avoidance defective worm strain CB3323 was used as a control for the Osm phenotype. Population chemotaxis to odorants assays were performed as described previously (Bargmann *et al*., 1993) using diacetyl (10^{-3} dilution), pyrazine (10^{-3} dilution), and isoamyl alcohol (10^{-3} dilution) as volatile attractants. The chemotaxis-defective worm strain CB1033 was used as a control for the Odr phenotype.

Generation and Analysis of Green Fluorescent Protein (GFP) Expression Constructs

The entire intergenic region between *dyf-2* and *cul-2*, including the first codons of both genes, was amplified and fused in both directions with the GFP gene of expression vector pPD95.77, respectively, resulting in *dyf-2::gfp* and *cul-2::gfp* transcriptional constructs. To produce a DYF-2::GFP translational fusion, 1 kb of promoter region plus full-length cDNA sequence of *dyf-2* were cloned into the pPD95.77 vector. To check for correct translational reading frames and promoter regions, all plasmid constructs were verified by sequencing. The translational DYF-2::GFP construct was introduced into a *dyf-2(m160)* mutant background and stable transgenic lines were analyzed for the rescue of *dyf-2* mutant phenotypes, by using, e.g., the dye-filling assay (Starich *et al*., 1995). For transgenesis, adult hermaphrodites were transformed using standard protocols (Mello *et al*., 1991). Constructs were injected typically at 10–100 ng/μl along with the coinjection marker pRF4 [contains the dominant marker *rol-6(su1006)*].

JT6924 and JT204 worm strains were used to test transcriptional constructs for GFP expression and dependence on *daf-19* function. The worm strain JT6924 *daf-19(m86); daf-12(sa204)* was used as a *daf-19* mutant background. Worms of this genotype exhibit a dauer larva formation-defective (Daf-d) phenotype and do not require the recovery of dauers. In this case, JT204 *daf-12(sa204)* worms were used as a wild-type background with regard to *daf-19*.

Microscopy and Imaging

GFP expression patterns were analyzed in stable transgenic lines at 1000× magnification by conventional fluorescence microscopy (Axioplan 2). Expression patterns were examined in at least two independent transgenic lines at most developmental stages of the worm. Determination of neuronal cell anatomies and identities followed published descriptions (Ward *et al*., 1975; White *et al*., 1986).

IFT was assayed as described previously (Orozco *et al*., 1999; Snow *et al*., 2004; Ou *et al*., 2005a). Transgenic worms anesthetized with 10 mM levamisole were mounted on agar pads and maintained at 21°C. Images were collected on an Olympus microscope equipped with a 100×, 1.35 numerical aperture objective and an Ultraview spinning disk confocal head at 0.3 s/frame for 2–3 min. Kymographs and movies were created using MetaMorph software (Molecular Devices, Sunnyvale, CA).

Antibody Production and Immunolocalization

A region of mouse WDR19 corresponding to amino acids 700 through 800 was amplified by reverse transcription-polymerase chain reaction from total mouse brain cDNA by using AccuTaq polymerase and cloned into the bacterial expression vector pET21b. The 6xHis-tagged WDR19 protein fragment was purified using nickel-nitrilotriacetic acid agarose according to the manufacturer's instructions (QIAGEN, Valencia, CA), and polyclonal antiserum was generated by Southern Biotechnology Associates (Birmingham, AL). To determine whether the immune serum was able to recognize endogenous WDR19, Western blot analysis was performed using lysate from cultured kidney inner medullary collecting duct (IMCD) cells. Confluent IMCD cells were lysed in a minimal volume of radioimmunoprecipitation assay buffer (150 mM NaCl; 1% NP-40; 1% SDS; 0.5% sodium deoxycholate; 50 mM Tris, pH 8.0, and equal amounts of protein were separated by SDS-PAGE and transferred to nitrocellulose. Western blots were probed using preimmune serum (diluted 1:10,000 in 5% dry milk in 0.1 M phosphate buffered saline [PBS]) or immune serum (diluted 1:10000 in 5% dry milk in PBS).

Immunolocalization was performed on cultured kidney IMCD cells and frozen tissue sections as described previously (Taulman *et al*., 2001; Haycraft *et al*., 2005). No specific staining was observed with preimmune serum. Nonaffinity purified antiserum was used for immunolocalization at a dilution of 1:1000 in 1% bovine serum albumin (BSA) in PBS. For blocking, antiserum was preincubated with at least a 10-fold molar excess of either 6xHis-tagged antigen or a nonspecific 6xHis-tagged protein in 1% BSA in PBS for 60 min at 4°C before incubation with tissue sections. Images of blocked and nonspecific blocked samples were imaged using identical settings and processing. Anti-acetylated α-tubulin antibodies were obtained from Sigma-Aldrich (St. Louis, MO). Nuclei were stained with Hoechst 33258. Images were captured on a Nikon TE200 Eclipse inverted epifluorescence microscope equipped with a CoolSnap HQ cooled charge-coupled device camera and MetaMorph software. All filters and shutters were computer driven.

RESULTS

Identification, Cloning, and Characterization of the dyf-2 Gene

To find the candidate gene for *dyf-2*, we used our knowledge about the X-box, a promoter motif located upstream of many ciliary genes, so-called *xbx* genes (Efimenko *et al*., 2005; Blacque *et al*., 2005). The gene ZK520.3, identified as a potential *xbx* gene candidate in our previous computational X-box searches, maps close to the genetic position of *dyf-2* (21.57 ± 0.320 cM) on linkage group III (Starich *et al*., 1995). Cosmid ZK526, which also maps to this region and contains the predicted ORF for ZK520.3, rescues the Dyf phenotype in *dyf-2*(*m160*) worms (Figure 1, B and C). Previously, it has been shown that the ZK520.3 predicted protein matches with the N-terminal end of human WDR19, whereas the C terminus of WDR19 corresponds to the neighboring ZK520.1 sequence in *C. elegans* (Lin *et al*., 2003). To show that both ZK520.3 and ZK520.1 predicted ORFs actually originate from one gene, we performed a screen of a *C. elegans* cDNA library and isolated the entire coding sequence, consisting of 19 exons (Figure 1A) (GenBank accession DQ314286). Further experiments demonstrated that the full-length cDNA can rescue dye-filling defects in mutants, confirming the identity of the *dyf-2* gene (our unpublished data).

The sequence of the DYF-2 protein was examined for the presence of conserved domains. Using SMART and Pfam databases, we have found that DYF-2 contains seven WD40 repeats (Figure 1A). Repeating WD40 units are thought to serve as a scaffold for protein interactions, which can occur simultaneously with several different proteins (Smith *et al*., 1999). Apart from WD repeats, DYF-2 contains three conserved tetratricopeptide repeats (TPRs) and one clathrin heavy chain repeat (CHCR), which also play important roles in protein–protein interactions (D'Andrea and Regan, 2003) and in endocytosis (Rappoport *et al*., 2004), respectively (Figure 1A).

We further characterized two available mutant alleles of *dyf-2* (Figure 1A). The reference allele, *m160*, affects cosmid ZK520-nt 10315 (C-to-T substitution converting R27 to a stop codon). *m160* thus most likely represents a functional null allele. The *m543* allele was obtained by spontaneous mutagenesis from the mutator strain RW7097 (Starich *et al*., 1995). Sequencing of this allele revealed a Tc1 transposon insertion within the last exon of the gene (cosmid ZK525-nt 19212/19213). Together with the transgenic rescue data, the identification of sequence alterations in two independent mutant alleles confirms that the combined ZK520.3 and ZK520.1 ORFs encode the gene *dyf-2*.

Generally, dye-filling defects are accompanied by various sensory mutant phenotypes, among them Osm, Che, Odr, Age, and so on (Starich *et al*., 1995; Munoz and Riddle, 2003). Accordingly, *dyf-2* mutant worms also have problems with avoidance of high osmolarity and odorant recognition. *dyf-2*(*m160*) mutants display a strong Osm phenotype; 90% of worms were able to cross a ring of 8 M glycerol in a 10-min assay, whereas complete rescue of the Osm phenotype was observed in *dyf-2*(*m160*) animals expressing a translational DYF-2::GFP fusion (Figure 1D). *dyf-2* mutants also exhibit defects in odorant recognition. We detected strongly impaired chemotaxis responses to volatile odorants such as pyrazine and iso-amyl alcohol, whereas the response to diacetyl was reduced to a lesser extent (Figure 1D). In summary, our results indicate that loss of *dyf-2* can lead to structural and functional abnormalities in ciliated sensory neurons.

Expression pattern and Transcriptional Regulation of dyf-2 in C. elegans

To determine the expression pattern of *dyf-2* in *C. elegans*, we generated a transcriptional *dyf-2::gfp* construct under the control of the entire *dyf-2* 5′ regulatory region (also see below). Surprisingly, *dyf-2::gfp* expression was observed in only a subset of the ciliated sensory neuron (CSN) class in the worm. We observed GFP signal in 7 of 12 neurons of the amphids, including ASH, ASI, ASJ, ASK, ADL (ciliated neurons that fill with the fluorescent dye DiI) plus two hitherto unidentified amphid neurons (Figure 2A). In addition, GFP expression was observed in the phasmid CSN and in neurons identified as AQR and PQR (asymmetric CSN in the head and tail, respectively). No or only very occasional GFP signal was detected in other CSN anterior to the nerve ring in the head of the worm. A translational DYF-2::GFP fusion was found to be localized only in cilia of CSN (Figure 4A), thus precluding a confirmation of the cellular expression pattern obtained with the transcriptional *dyf-2::gfp* fusion or any further cell identification.

The promoter region of *dyf-2* contains an X-box sequence motif (Table 1 and Figure 2C). Intriguingly, the *dyf-2* gene shares its promoter region with the neighboring gene *cul-2*. Because the X-box is a near-palindrome sequence motif and the promoter region is relatively short (~1.3 kb), it is possible that DAF-19, the X-box binding transcription factor (Swoboda *et al*., 2000), can affect the expression of both genes. To examine this possibility, we fused the promoter sequence to GFP in two different directions, both for *dyf-2* and *cul-2* (Figure 2C). These two transcriptional fusions

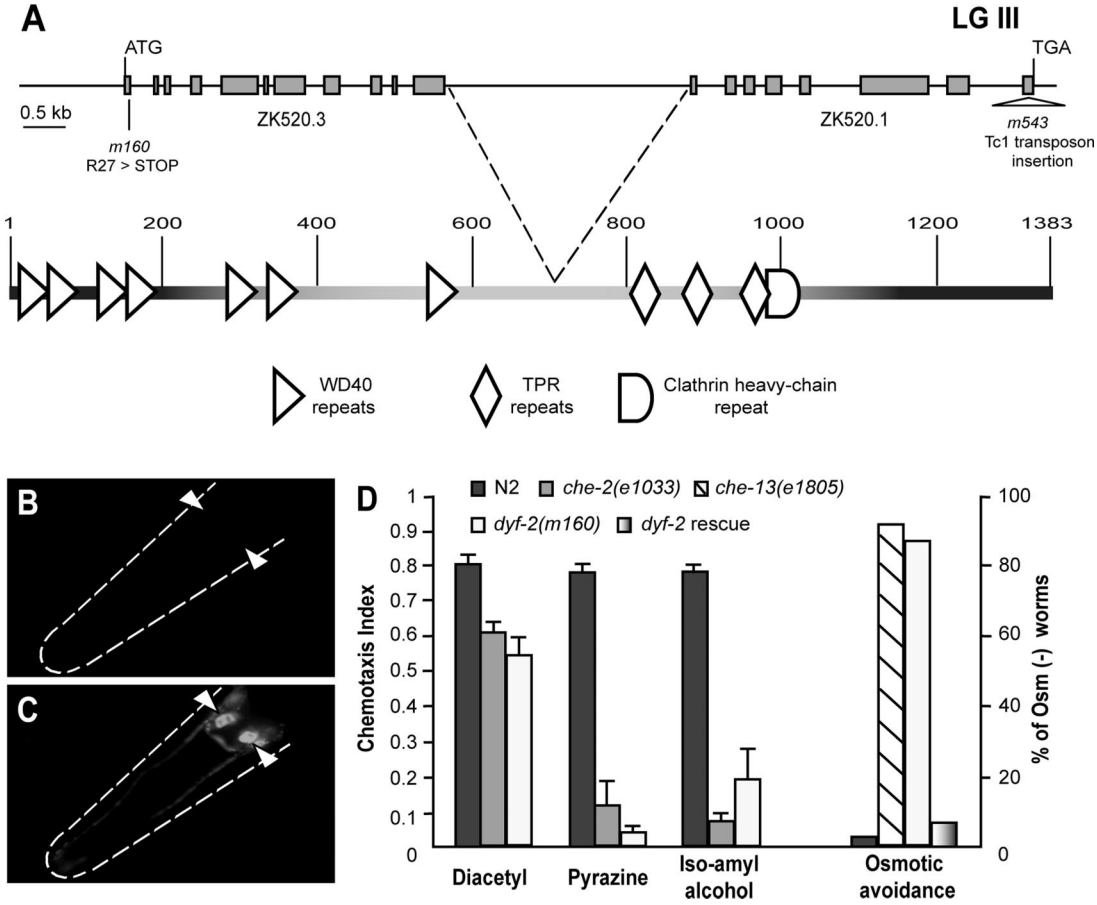

Figure 1. Molecular characterization of the *dyf-2* gene. (A) Genomic organization of the *dyf-2* gene on linkage group III. Gray boxes depict exons. The coding sequence consists of 19 exons and covers two predicted ORFs, ZK520.3 and ZK520.1. There are two different *dyf-2* mutant alleles. The *m160* allele contains a C-to-T substitution in the first exon converting R27 to a stop codon. The *m543* mutation was found to be a Tc1 transposon insertion in the last exon of the gene. *dyf-2* encodes a large protein of 1383 amino acids. Conserved domains and repeats within the protein sequence are indicated. Dye-filling defects of *dyf-2*(*m160*) mutants (B) can be rescued in transgenic worms by injections of ZK525 cosmid or full-length *dyf-2* cDNA (C). Positions of dye-filling neurons are indicated with arrowheads in mutant (B) and rescued (C) animals. The outline of the worm head is depicted by a dashed line in both panels. (D) *dyf-2*(*m160*) mutant worms show defects in chemotaxis toward different odorants and in avoidance of high osmolarity.

were introduced into wild-type and *daf-19* mutant backgrounds. Transgenic worms were subsequently analyzed for their expression patterns. CSN-specific expression of the *dyf-2::gfp* fusion was absent or dramatically reduced in *daf-19* mutant worms (Figure 2B), whereas the expression of *cul-2::gfp* was DAF-19 independent and observed mostly in hypodermal seam cells (our unpublished data). These data confirm our previous model, where the position of the X-box sequence motif relative to the gene start is crucial for proper activation of the target in CSN (Efimenko *et al*., 2005).

Putative orthologues of DYF-2 were identified in many different species, including *Drosophila*, mouse, and human (Table 2) (Lin *et al*., 2003; Avidor-Reiss *et al*., 2004). The presence of the X-box sequence motif is highly conserved in promoters of different *dyf-2* orthologues and typically matches well to the refined *C. elegans* consensus (Table 1), suggesting a common regulatory mechanism of transcription.

The Mouse Orthologue of DYF-2, WDR19, Colocalizes with Cilia in Higher Organisms

Hints about the possible role of mammalian WDR19 in ciliogenesis come from our work and from expression data of its *Drosophila* orthologue, the gene *oseg6* (Table 2) (Avidor-Reiss *et al*., 2004). To determine whether the ciliary localization of DYF-2/WDR19 is conserved in higher organisms, we generated polyclonal antiserum against the murine WDR19. To verify that the immune serum specifically recognized the endogenous WDR19, we performed Western blot analysis on total lysate from cultured kidney IMCD cells. Anti-WDR19 immune serum specifically recognized a protein of ~145 kDa, the predicted molecular mass of murine WDR19, that was not recognized by preimmune serum (Figure 3A).

To determine the subcellular localization of WDR19, we performed immunofluorescent staining on frozen tissue sections and IMCD cells. The ependymal cells lining the ventricles of the brain express multiple motile cilia that protrude into the ventricle as visualized by the localization of acetylated α-tubulin immunostaining (Figure 3, B and C). WDR19 immunostaining was observed prominently at the base of the cilia of the ependymal cells (Figure 3B). To verify that the localization pattern seen was specific for WDR19, the antiserum was preincubated with an excess of the immunizing antigen or a nonspecific protein before incubation with tissue sections. Preincubation of the immune serum with the WDR19 antigen but not a nonspecific protein blocked the immunofluorescence signal in the cilia (Figure 3C). Colocal-

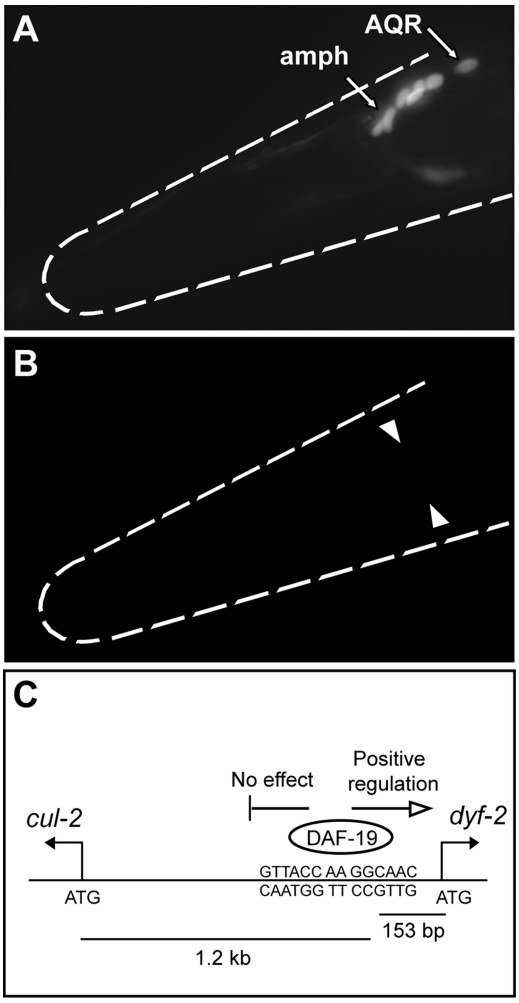

Figure 2. Expression properties of *dyf-2* in *C. elegans*. (A) *dyf-2::gfp* is expressed in a subset of CSNs. Typically, expression was observed in some neurons of the amphids (amph) and in the phasmids (our unpublished data). (B) In a *daf-19* mutant background expression of *dyf-2* was dramatically reduced or absent. Arrowheads indicate positions of amphid sensory neuron cell bodies. The outline of the worm head is depicted by a dashed line in both panels. (C) *dyf-2* shares its promoter region with the neighboring gene *cul-2*. However, the ciliogenic transcription factor DAF-19 regulates only the expression of *dyf-2*, suggesting the importance of X-box promoter motif position relative to its target gene.

ization of WDR19 and acetylated α-tubulin was also observed in the primary cilia of cultured murine IMCD cells, whereas staining with preimmune serum showed no specific signal (Figure 3, D and E). Our immunostaining data suggest that ciliary expression of DYF-2/WDR19 is conserved in higher organisms. Furthermore, the presence of the protein both in motile and sensory cilia in mammals further suggests a universal role of DYF-2/WDR-19 in the formation of ciliated structures.

DYF-2 Protein Shows Biphasic Movements within Cilia

To explore the possible role of DYF-2 in the development of ciliated structures, we generated transgenic worm strains carrying a DYF-2::GFP translational fusion. We could clearly demonstrate a specific localization of protein in ciliated endings of sensory neurons (Figure 4A). Transgenic worms

Table 1. Conservation of the X-box sequence motif in promoter regions of different *dyf-2* orthologues

Species	Position upstream of the ATG	X-box sequence[a]
C. elegans	−153	GTTACC AA GGCAAC
C. briggsae	−136	GTTGCT AT GGA**T**AC
D. melanogaster	−91	G**C**TACC AT GGAAAC
Mouse	−1348	ATCCCT A**A** GAT**C**AC
Human	−1535[b]	GTCTT**G** TT AAGAAC
Refined consensus		RTHNYY WT RRNRAC

[a] R, G or A; Y, C or T; H, A or C or T; W, A or T; and N, any nucleotide. Bold denotes a mismatch to the refined X-box consensus in *C. elegans* (Efimenko *et al*., 2005).

[b] Position is given relative to a weak start codon according to Lin *et al*. (2003).

carrying the DYF-2::GFP transgene were also able to absorb fluorescent dye (our unpublished data) in a *dyf-2* mutant background, confirming that the translational DYF-2::GFP fusion is fully functional. Using time-lapse spinning disk confocal microscopy we observed DYF-2::GFP fluorescent particles moving along the ciliary axoneme (Supplemental Movie S1). Further analysis of kymographs revealed that DYF-2 molecules move with different velocities in the anterograde direction along the middle (0.68 ± 0.10 μm/s) and distal (1.25 ± 0.12 μm/s) segments of the cilium (Figure 4A, Table 3, and Supplemental Movie S1). These data are in agreement with previously described velocities for other IFT proteins such as CHE-2, OSM-5, or OSM-6 as well as BBS proteins (Snow *et al*., 2004, Ou *et al*., 2005a). Together, these observations suggest that DYF-2 is involved in the process of IFT as a component of IFT particles, which are driven biphasically by the cooperative action of kinesin-II and OSM-3-kinesin motors (Snow *et al*., 2004, Ou *et al*., 2005a).

Ciliary Defects in dyf-2 Mutants

dyf-2 mutants show defects in fluorescent dye filling (Dyf), indicative of cilium structure abnormalities (Starich *et al*., 1995). To visualize these abnormalities in detail, we used GFP markers that are specifically expressed in CSNs. We analyzed cilium morphology of specific amphid and phasmid CSN by using *bbs-7::gfp* and *srh-142::gfp* transcriptional fusions as fluorescent markers. We found that cilia structures of *dyf-2*(*m160*) animals were significantly shorter in comparison with wild-type controls (Figure 4, C and D; our unpublished data). The average length of phasmid cilia was 6.97 μm in wild-type worms, whereas in mutants it was significantly reduced to 2.84 μm, leaving only the transition zone and a short part of the middle segment.

Ciliary abnormalities in different IFT mutants have been analyzed in detail. Mutations affecting proteins that function as part of IFT particle complex A or B, display characteristic, distinct morphologies. Thus, the ciliary axoneme in complex B mutants is significantly shorter than that of complex A mutants (Perkins *et al*., 1986; Qin *et al*., 2001; Haycraft *et al*., 2003; Schafer *et al*., 2003). Our analysis of *dyf-2*(*m160*) mutant worms demonstrated that their cilium morphology closely resembles the short ciliary stumps observed in complex B mutants (Figure 4, C and D). Therefore, these data further

Table 2. Cross-species comparison of WDR genes involved in ciliogenesis

Gene name or gene model in *C. elegans*	Gene name or gene model in *D. melanogaster*	Gene name or gene model in human
daf-10 (F23B2.4) (Qin *et al*., 2001)	*oseg1* (CG7161) (Avidor-Reiss *et al*., 2004)	*WDR10* (Gross *et al*., 2001)
osm-1 (T27B1.1) (Signor *et al*., 1999b)	*oseg2* (CG13809) (Avidor-Reiss *et al*., 2004)	*SLB* (Howard and Maurer, 2000)
che-11 (C27A7.4) (Qin *et al*., 2001)	*oseg3* (CG11838) (Avidor-Reiss *et al*., 2004)	KIAA0590 (uncharacterized)
C54G7.4 (Blacque *et al*., 2005)	*oseg4* (CG2069) (Avidor-Reiss *et al*., 2004)	*WDR35* (uncharacterized)
che-2 (F38G1.1) (Fujiwara *et al*., 1999)	*oseg5* (CG9333) (Avidor-Reiss *et al*., 2004)	*WDR56* (uncharacterized)
dyf-2 (ZK520.3/1) (this work)	*oseg6* (CG11237) (Avidor-Reiss *et al*., 2004)	*WDR19* (Lin *et al*., 2003)

suggest that DYF-2 is involved in IFT and can associate with particle complex B (also see below).

Localization of DYF-2::GFP Fluorescent Particles in Different IFT Mutant Backgrounds

Specific ciliary abnormalities exhibited by *dyf-2* mutants together with the localization and movement of fluorescence-tagged DYF-2 demonstrate that this protein functions in IFT. To find out at which point DYF-2 molecules are necessary for proper IFT to occur, we placed the DYF-2::GFP protein in different IFT mutant backgrounds. In previous studies it was shown that the assembly of IFT complexes occurs in a sequential manner (Baker *et al*., 2003; Haycraft *et al*., 2003; Schafer *et al*., 2003; Lucker *et al*., 2005). Therefore, expression of fluorescence-tagged DYF-2 in the context of IFT complex A or B mutants could illuminate the hierarchy with which the protein functions in IFT particle assembly.

The gene *che-11* encodes a well-defined member of IFT particle complex A (Qin *et al*., 2001; Ou *et al*., 2005a). In *che-11* mutants, DYF-2::GFP was observed within swollen cilia (Figure 4E), suggesting that a complex A protein like CHE-11 is likely not important for the ability of DYF-2 to enter cilia or the assembly of IFT particles at ciliary transition zones.

In a *che-13* mutant background, representing IFT particle complex B (Haycraft *et al*., 2003), DYF-2::GFP accumulated only around the transition zone and could not enter into residual cilia (Figure 4F). These data indicate the importance of CHE-13 protein for the proper localization of DYF-2 molecules. It might also suggest that DYF-2 is located downstream of CHE-13 within the hierarchy of IFT particle complex B assembly (Figure 6).

Finally, we moved DYF-2::GFP into a *bbs-8* mutant background. It has been shown that BBS proteins play important roles in the assembly of IFT particles and in the functional coordination of two anterograde IFT-kinesins (Blacque *et al*., 2004; Ou *et al*., 2005a). IFT particles in *bbs-7* and *bbs-8* mutants break down into two subcomplexes, IFT-A and IFT-B, which are moved separately by kinesin-II and OSM-3-kinesin, respectively (Ou *et al*., 2005a). In *bbs-8(nx77)* mutants, DYF-2::GFP fluorescent particles move with a unitary fast rate along the middle (1.09 $\pm$ 0.13 μm/s) and distal (1.33 $\pm$ 0.12 μm/s) segments of the cilium, which is characteristic of OSM-3-kinesin–directed movement (Ou *et al*., 2005a) (Figure

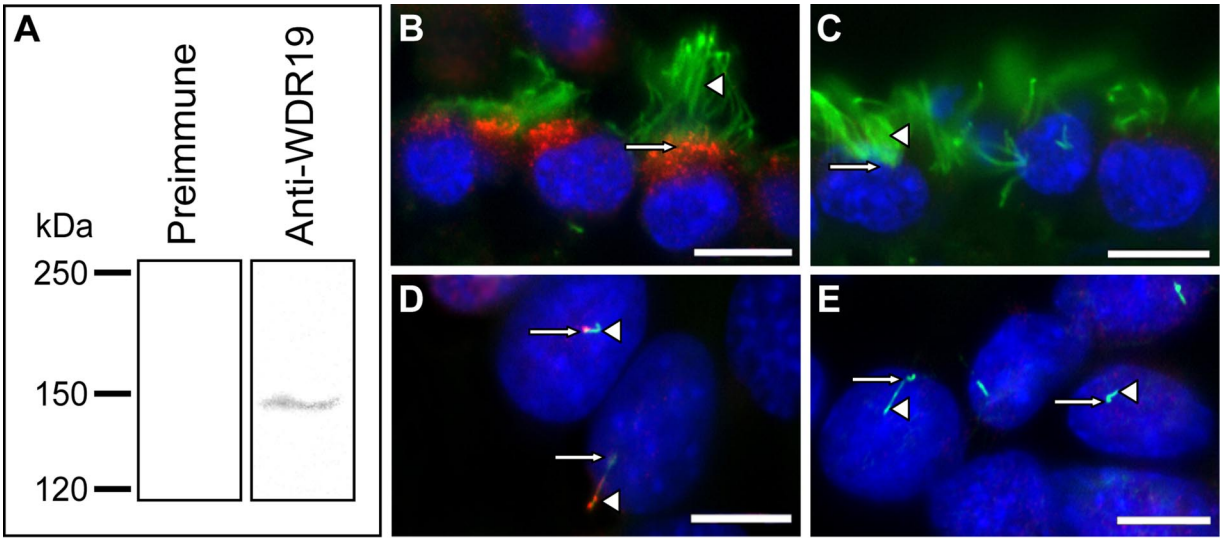

Figure 3. Immunolocalization of mouse WDR19 to cilia. (A) The WDR19 immune serum recognized a protein of ~145 kDa, the predicted molecular mass of endogenous WDR19, from cultured kidney IMCD cell lysate by Western blot analysis. (B) In the ependymal cells lining the ventricles of the mouse brain, WDR19 (red) localizes to the base of motile cilia as identified by staining with acetylated α-tubulin (green) and is unaffected by preincubation of the immune serum with an excess of nonspecific protein. (C) Preincubation of the WDR19 antiserum with an excess of immunizing protein results in a loss of immunostaining at the base of cilia (green) in the ependymal cells. (D) Staining of cultured kidney IMCD cells with immune serum showed localization of WDR19 (red) at the base of and along the primary cilium, identified by staining with anti-acetylated alpha-tubulin (green). (E) In contrast, no specific staining was detected when cultured IMCD cells were incubated with preimmune serum. Nuclei are blue in all panels. Arrowheads indicate ciliary axonemes. Arrows indicate ciliary base. Scale bars, 10 μm.

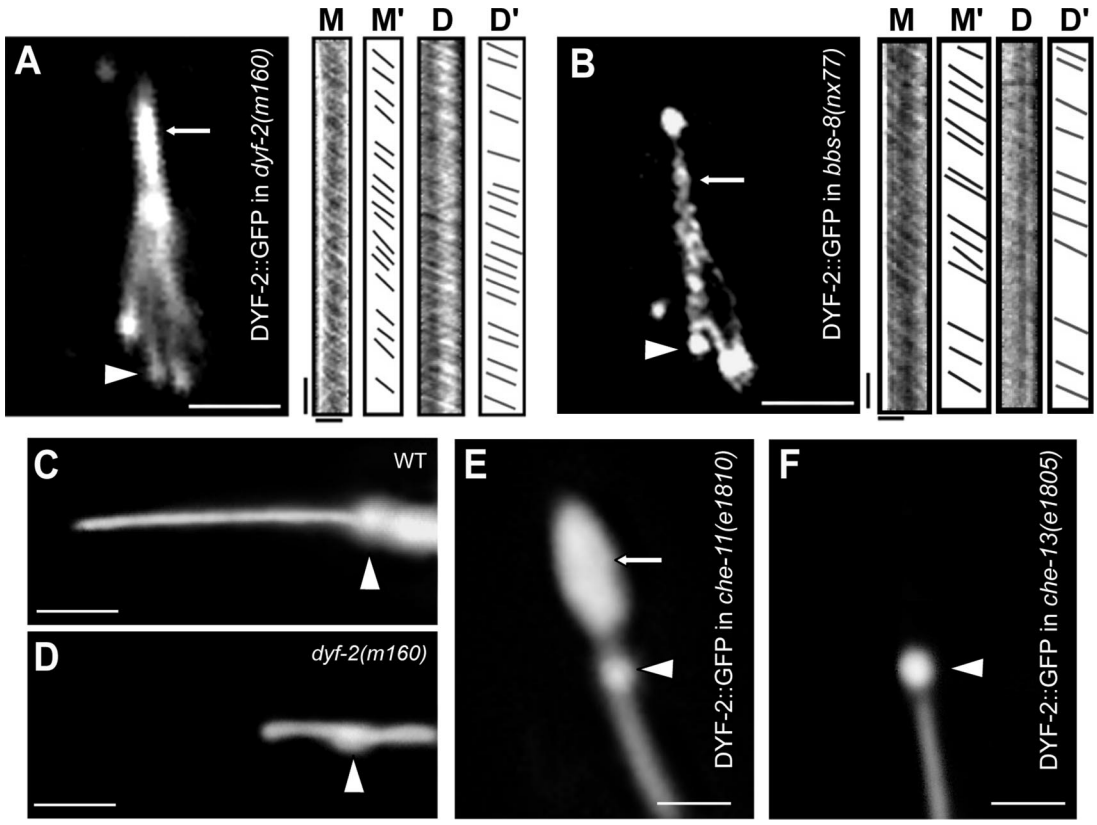

Figure 4. DYF-2 associates with IFT particle complex B. (A) Motility of DYF-2::GFP fluorescent particles within cilia. Fluorescent micrograph (left) and kymographs with corresponding cartoons (right) showing specific localization of DYF-2::GFP within amphid cilia and indicating trajectories of moving particles along middle (M, M′) and distal (D, D′) segments. (B) Motility of DYF-2::GFP fluorescent particles within the amphid cilia of *bbs-8* mutants. Scale bars (A and B), 5 μm; kymograph horizontal bars, 2.5 μm; vertical bars, 5 s (also see Table 3 and Supplemental Movies S1 and S2). (C and D) Morphology of the phasmid cilium in wild-type (C) and *dyf-2* mutant (D) backgrounds. Scale bars, 2 μm. (E and F) Localization of DYF-2::GFP fluorescent particles in phasmid cilia of *che-11* (IFT-A) (E) and *che-13* (IFT-B) (F) mutant backgrounds. Arrowheads indicate ciliary transition zones. Arrows indicate ciliary axonemes.

4B, Table 3, and Supplemental Movie S2). The obtained movement data, which are similar to those observed for IFT-B proteins (OSM-5, OSM-6, or CHE-2), suggest that DYF-2 can associate with IFT-particle complex B.

Effects of the dyf-2 Mutation on the Behavior of Other IFT Proteins

To further evaluate the possibility that DYF-2 functions in IFT, we expressed different members of this complex (OSM-5, OSM-6, CHE-13 [all IFT-B], and CHE-11 [IFT-A]) in the context of a *dyf-2* mutant background. These IFT proteins were properly localized in wild-type cilia (Figure 5, A–C), whereas in cilia of *dyf-2* mutants they displayed different degrees of mislocalization. The localization of CHE-11 protein was restricted to transition zones of cilia in a *dyf-2* mutant background (Figure 5F), pointing toward an interaction of DYF-2 with components of complex A. OSM-5 is a previously characterized IFT-B protein, which was predicted to function downstream of CHE-13 in the IFT assembly process (Haycraft *et al*., 2001; Haycraft *et al*., 2003). When introduced into a *dyf-2* mutant background, OSM-5::GFP was no longer located at the base of cilia and was diffusely spread throughout the dendrites (Figure 5D), indicating that DYF-2 is required for ciliary loading of OSM-5 molecules. Unlike OSM-5::GFP, both CHE-13::YFP and OSM-6::GFP could enter and accumulate in residual cilia of *dyf-2* mutants,

Table 3. Velocities of DYF-2 molecules in *dyf-2* and *bbs-8* mutant backgrounds

		Average velocities ($\mu m\ s^{-1}$)			
Anterograde motility of	Strain genotype	Middle segment	n	Distal segment	n
DYF-2::GFP	*dyf-2*(*m160*)	0.68 ± 0.10	105	1.25 ± 0.12	106
	bbs-8(*nx77*)	1.09 ± 0.13	105	1.33 ± 0.12	80

n, number of GFP particles analyzed. Also see Figure 4, A and B, and Supplemental Movies S1 and S2.

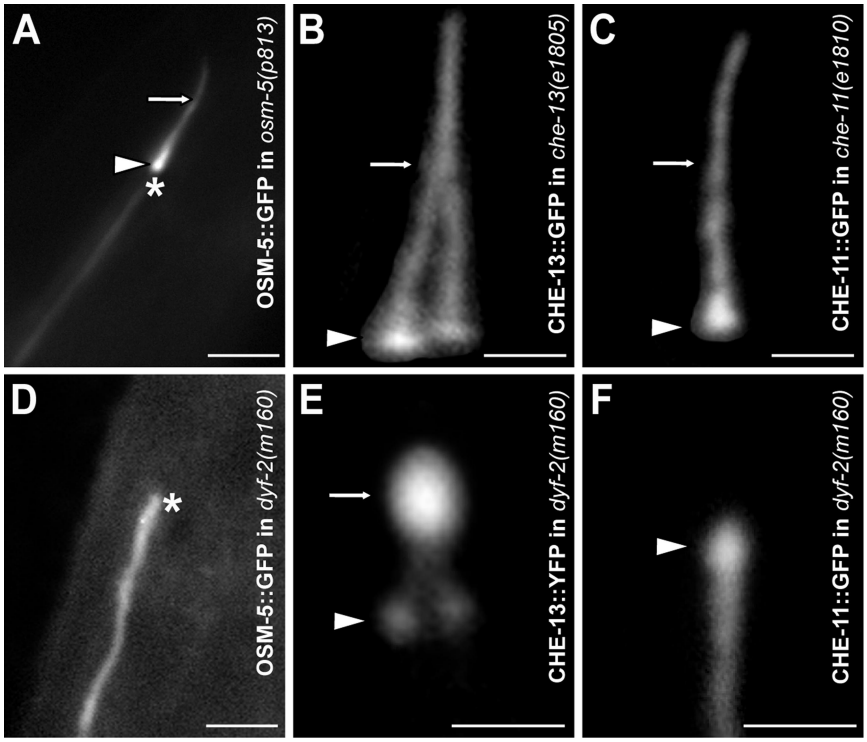

Figure 5. Localization of fluorescence-tagged IFT proteins in phasmid cilia of control and *dyf-2* mutant worms. (A–C) Localization of fluorescence-tagged IFT proteins (OSM-5, CHE-13, and CHE-11) in wild-type cilia. In a *dyf-2* mutant background OSM-5 (IFT-B) (D) is diffusely localized throughout the dendrites and not localized in cilia, whereas CHE-13 (IFT-B) (E) accumulates in residual cilia. (F) CHE-11 (IFT-A) localizes at the transition zone and cannot enter the ciliary axoneme in a *dyf-2* mutant. Arrowheads indicate ciliary transition zones. Arrows indicate ciliary axonemes. The dendrite ending is marked with an asterisk. Scale bars, 5 μm (A and D) and 2 μm (B, C, E, and F).

also suggesting abnormalities in retrograde transport (Figure 5E; our unpublished data for OSM-6). The observation of ciliary accumulations was rather surprising considering that abnormalities in retrograde transport were previously observed only in complex A or dynein mutants (Haycraft *et al*., 2003; Schafer *et al*., 2003). A recent model of IFT in *Chlamydomonas* suggests that components of complex B are indeed required for targeting of intact dynein molecules, the retrograde motor, to the flagellum (Pedersen *et al*., 2006).

Summarizing all of the aforementioned information, we show that DYF-2 is a novel component of the IFT machinery that acts downstream of CHE-13 and OSM-6 but upstream of OSM-5 within the hierarchy of particle complex B. At the same time, mutations in *dyf-2* can interfere with the function of complex A components, suggesting an important role of this protein for the assembly of the IFT particle as a whole (Figure 6).

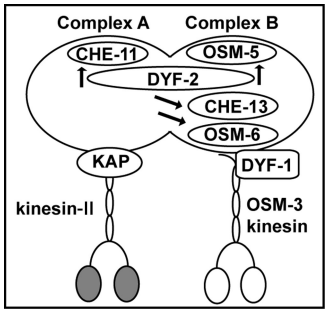

Figure 6. Hypothetical model for the role of DYF-2 within the IFT particle. The assembly of the IFT particle occurs through an ordered process, where DYF-2 can associate with IFT particle complex B after CHE-13 and OSM-6. DYF-2 function is required before OSM-5. While associating with complex B, DYF-2 molecules can also interfere with the function of components from complex A, like CHE-11, or selectively affect the retrograde motility of some complex B components. Note that not all known *C. elegans* IFT components are shown in this figure.

DISCUSSION

With the long-term aim of elucidating the genetic mechanisms of ciliogenesis, *C. elegans* mutants have been generated where the CSNs of the amphids and phasmids are rendered fluorescent dye-filling defective (*dyf* mutants) (Starich *et al*., 1995), the Dyf phenotype being indicative of general defects in cilium structure. In our previous studies, we have shown that *C. elegans* genes of cilium structure typically contain an X-box sequence motif in their promoters (*xbx* genes) (Swoboda *et al*., 2000; Fan *et al*., 2004; Efimenko *et al*., 2005; Blacque *et al*., 2005). Three recent papers describe the X-box sequence motif as an additional tool to determine the molecular identities of the ciliary genes *dyf-1*, *dyf-3*, and *dyf-13* (Blacque *et al*., 2005; Murayama *et al*., 2005; Ou *et al*., 2005a). In our work, we used X-box position across the *C. elegans* genome in combination with genetic map data for determining the identity of *dyf-2*. As a result, we were able to clone *dyf-2* just by means of a single transgenic rescue experiment, which makes our approach very valuable for cloning the rest of the members from the *dyf* gene class.

Most of the identified *dyf* genes encode proteins, which are part of or associated with IFT (Blacque *et al*., 2005; Murayama *et al*., 2005; Ou *et al*., 2005a). Biochemically defined in *Chlamydomonas*, *C. elegans* IFT proteins fall into two different complexes based on ciliary phenotypes of their mutants. Complex B mutants typically show severely reduced cilia where other IFT particle components fail to enter and migrate from the base to the distal tip of the cilia, but rather they accumulate at transition zones, supporting a role of IFT-B components in anterograde transport (Perkins *et al*., 1986; Haycraft *et al*., 2003; Schafer *et al*., 2003). Cilia of IFT-A

mutants are only slightly stunted and show a bulb-like structure at the distal tip with massive accumulation of IFT proteins along the axoneme, indicating the importance of IFT-A for retrograde transport (Perkins *et al*., 1986; Qin *et al*., 2001; Schafer *et al*., 2003). Another criterion that helps to distinguish between complexes A and B was obtained from studies of *C. elegans bbs* mutants. Previously, fluorescence-tagged components of IFT-A and IFT-B subunits have been observed moving together, albeit at different speeds along the middle and distal segments of the cilium, respectively (Ou *et al*., 2005a). In *bbs-7* and *bbs-8* mutant backgrounds, however, complex A components move only in the middle and not the distal ciliary segments at the same rate as kinesin-II, whereas complex B components move in both ciliary segments at the faster rate of OSM-3-kinesin (Ou *et al*., 2005a).

To find the possible role of *dyf-2* during ciliogenesis, we applied experimental approaches such as cilia length measurements in *dyf-2* mutants, expression of DYF-2::GFP in *bbs* and in two different IFT (A and B) mutant backgrounds as well as expression of other IFT proteins in a *dyf-2* mutant background. The results obtained suggest that DYF-2 protein can function in the process of intraflagellar transport associated with IFT particle complex B. However, expression of IFT-B components (OSM-6 or CHE-13) in a *dyf-2* mutant background leads to their accumulation within residual cilia, suggesting abnormalities in retrograde transport. This observation was rather surprising, considering the role of IFT-B proteins in anterograde transport. Therefore, we suggest that in addition to its involvement in complex B, DYF-2 molecules can also interfere with complex A components or selectively affect the retrograde motility of some complex B components (Figure 6). Further experiments are needed to fully investigate the possible involvement of DYF-2 in the process of IFT retrograde transport.

The IFT particle composition is very similar between *C. elegans* and *Chlamydomonas*. IFT assembly is an ordered process that requires multiple protein–protein interactions, as confirmed by our DYF-2 data. However, using biochemical techniques, IFT88 is associated with the core of complex B in *Chlamydomonas* (Lucker *et al*., 2005), whereas its *C. elegans* orthologue OSM-5 is rather associated with the periphery of IFT-B, as shown by genetic and cell biological analyses (Haycraft *et al*., 2003; this work). It is presently unclear whether these differences found between *C. elegans* and *Chlamydomonas* could be due to different experimental approaches, to different physiological stabilities of IFT complexes, or to potentially different mechanisms of particle complex assembly between sensory cilia and motile flagella.

Whereas many known IFT-B genes (*osm-1*, *osm-5*, *osm-6*, *che-2*, or *che-13*) are expressed in most or all CSNs, the expression of a transcriptional *dyf-2::gfp* fusion was observed in only a subset of CSNs. This observation might be indicative of specialized properties of DYF-2 within the IFT particle complex. Sensory cilia in *C. elegans* consist of three sections. The proximal segment is ~1 μm in length and can be considered as the functional equivalent of a transition zone. The middle segment contains ~4-μm doublet microtubules that lead to a distal segment of ~2.5-μm singlet microtubules (Perkins *et al*., 1986; Snow *et al*., 2004). The IFT motors kinesin-II and OSM-3-kinesin cooperate to form two sequential anterograde IFT pathways that build distinct parts of cilia in the worm: a middle segment pathway driven by kinesin-II and OSM-3 together and a distal segment pathway driven by OSM-3 alone. It has been shown that OSM-3 is exclusively expressed in a subset of ciliated neurons that is responsible for chemosensation (Tabish *et al*., 1995). Thus, we hypothesize that some IFT proteins are important for the general formation of cilia, whereas others are necessary for the development of specialized cilia structures. Considering the similarity in expression patterns between *dyf-2* and *osm-3*, DYF-2 could thus be required for only the distal segment pathway, mediated by OSM-3-kinesin. Studies of DYF-3/Qilin, a conserved IFT protein that is expressed in only a subset of CSNs, are also suggestive for specializations during the development of ciliated structures (Murayama *et al*., 2005). The *dyf-2* expression pattern also fits a model that sorts ciliary genes with an X-box promoter motif (*xbx* genes) into two groups, where members of group 1 are typically required for more general aspects of cilia formation, whereas genes from group 2 are typically required for more specialized functions within cilia and/or CSNs (Efimenko *et al*., 2005). *dyf-2* contains an asymmetric X-box sequence motif (GTTACC **AA** GGCAAC), which fits Group 2 *xbx* genes, and probably requires for regulation some cell specific factors in addition to DAF-19, the ciliogenic transcription factor binding to the X-box (Swoboda *et al*., 2000).

Like many other IFT proteins, DYF-2 contains prominent WD40 and TPR repeats. WD40-containing proteins are thought to fold into a β-propeller structure and to coordinate multiprotein complex assemblies (Smith *et al*., 1999). IFT particle assembly could serve as an example for such complexes (Table 2). TPR motifs occur as 3–16 tandem repeats per protein that are packed in a parallel manner and form a superhelical structure for interaction with a diverse range of target proteins (D'Andrea and Regan, 2003). For example, WD40 repeats in IFT proteins are accompanied by TPRs (Table 2), although some IFT proteins such as OSM-5 are composed of only TPR repeats (Haycraft *et al*., 2001). Apart from WD40 and TPR repeats, DYF-2 contains one CHCR, which is characteristic for proteins of clathrin-coated vesicles (Rappoport *et al*., 2004). According to a recent model for the evolution of IFT, nonvesicular, membrane-bound IFT could have evolved as a specialized form of coated vesicle transport from a protocoatomer complex (Jekely and Arendt, 2006).

Defined by the presence of four or more repeating units containing a conserved core of ~40 amino acids that usually end with WD, the WDR protein family comprises a large group of functionally distinct but structurally related proteins (Li and Roberts, 2001). The functions of some identified WDR proteins range from signal transduction to cell cycle control, whereas for others, the function remains unknown. The first insight into their possible roles in ciliogenesis was obtained from studies of WDR orthologues in *C. elegans*. Mutations in *C. elegans WDR* genes lead to varieties of structural and functional abnormalities of sensory cilia. It has been shown that most of them are involved in IFT (Fujiwara *et al*., 1999; Signor *et al*., 1999b; Qin *et al*., 2001) (Table 2). Later, the expression patterns and some mutants of *WDR* genes have been analyzed in *Drosophila melanogaster* (Avidor-Reiss *et al*., 2004). These genes were specifically required for the cilia outer segment formation (*oseg* genes) (Table 2). The identification of several *WDR* genes, including *WDR19*, has also been described in humans (Howard and Maurer, 2000; Gross *et al*., 2001; Lin *et al*., 2003) (Table 2). In our current work, we demonstrate that the function of DYF-2, the *C. elegans* orthologue of human WDR19, is required for proper cilia formation. We have shown that ciliary expression of DYF-2/WDR19 is conserved in mammals. Given this fact we predict a ciliogenic function also for some other members of this family in humans. For example, the expression of the human *SLB* and *WDR10* genes was abun-

dant in ciliated tissues such as testis or pituitary gland (Howard and Maurer, 2000; Gross *et al*., 2001). Moreover, *WDR10* is one of the candidate genes for retinitis pigmentosa 4, an inheritable human disease that causes progressive blindness (Gross *et al*., 2001). Apart from retinitis pigmentosa, defects in IFT can lead to a wide range of human syndromes and pathologies, including BBS, polycystic kidney disease, nephronophthisis, maturity-onset obesity, situs inversus, and hydrocephalus (Pazour and Rosenbaum, 2002; Rosenbaum and Witman, 2002; Scholey, 2003; Afzelius, 2004; Banizs et al., 2005). Therefore, the study of WDR proteins, like is the case for PKD and BBS proteins, will be important for the understanding of cilia-dependent events during development as well as cilia-dependent diseases.

ACKNOWLEDGMENTS

We thank the following people for technical assistance, helpful discussions, *C. elegans* strains, cosmid clones, cDNA clones, RNA interference clones, and GFP vectors: A. Coulson, A. Fire, D. Riddle, D. Baillie, T. Murayama, J. Burghoorn, and S. Dutcher. We thank the *C. elegans* Genome Sequencing Consortium for providing genome sequence information and the *Caenorhabditis* Genetics Center, which is funded by the National Institutes of Health, for providing some of the *C. elegans* strains used in this study. M.R.L. acknowledges funding from March of Dimes and Canadian Institutes of Health Research (CIHR; Grant CBM134736) and is supported by scholar awards from CIHR and Michael Smith Foundation for Health Research (MSFHR). O.E.B. is the recipient of an MSFHR fellowship award. This work was also supported by National Institutes of Health Grants T32 HL07553-22 to J. Yother (C.J.H.), R01 DK-62758 (B.K.Y.), and GM-50718 (G.O. and J.M.S.). Work in the laboratory of P.S. is supported by grants from the Swedish Research Council and from the Swedish Foundation for Strategic Research.

REFERENCES

Afzelius, B. A. (2004). Cilia-related diseases. J. Pathol. *204*, 470–477.

Avidor-Reiss, T., Maer, A. M., Koundakjian, E., Polyanovsky, A., Keil, T., Subramaniam, S., and Zuker, C. S. (2004). Decoding cilia function: defining specialized genes required for compartmentalized cilia biogenesis. Cell *117*, 527–539.

Baker, S. A., Freeman, K., Luby-Phelps, K., Pazour, G. J., and Besharse, J. C. (2003). IFT20 links Kinesin II with a mammalian intraflagellar transport complex that is conserved in motile flagella and sensory cilia. J. Biol. Chem. *278*, 34211–34218.

Banizs, B., Pike, M. M., Millican, C. L., Ferguson, W. B., Komlosi, P., Sheetz, J., Bell, P. D., Schwiebert, E. M., and Yoder, B. K. (2005). Dysfunctional cilia lead to altered ependyma and choroid plexus function, and result in the formation of hydrocephalus. Development *132*, 5329–5339.

Bargmann, C. I., Hartwieg, E., and Horvitz, H. R. (1993). Odorant-selective genes and neurons mediate olfaction in *C. elegans*. Cell *74*, 515–527.

Blacque, O. E., *et al*. (2004). Loss of *C. elegans* BBS-7 and BBS-8 protein function results in cilia defects and compromised intraflagellar transport. Genes Dev. *18*, 1630–1642.

Blacque, O. E., *et al*. (2005). Functional genomics of the cilium, a sensory organelle. Curr. Biol. *15*, 935–941.

Brenner, S. (1974). The genetics of *Caenorhabditis elegans*. Genetics *77*, 71–94.

Cole, D. G., Chinn, S. W., Wedaman, K. P., Hall, K., Vuong, T., and Scholey, J. M. (1993). Novel heterotrimeric kinesin-related protein purified from sea urchin eggs. Nature *366*, 268–270.

Cole, D. G., Diener, D. R., Himelblau, A. L., Beech, P. L., Fuster, J. C., and Rosenbaum, J. L. (1998). *Chlamydomonas* kinesin-II–dependent intraflagellar transport (IFT): IFT particles contain proteins required for ciliary assembly in *Caenorhabditis elegans* sensory neurons. J. Cell Biol. *141*, 993–1008.

Collet, J., Spike, C. A., Lundquist, E. A., Shaw, J. E., and Herman, R. K. (1998). Analysis of *osm-6*, a gene that affects sensory cilium structure and sensory neuron function in *Caenorhabditis elegans*. Genetics *148*, 187–200.

Culotti, J. G., and Russell, R. L. (1978). Osmotic avoidance defective mutants of the nematode *Caenorhabditis elegans*. Genetics *90*, 243–256.

D'Andrea, L. D., and Regan, L. (2003). TPR proteins: the versatile helix. Trends Biochem. Sci. *28*, 655–662.

Dutcher, S. K. (1995). Flagellar assembly in two hundred and fifty easy-to-follow steps. Trends Genet. *11*, 398–404.

Efimenko, E., Bubb, K., Mak, H. Y., Holzman, T., Leroux, M. R., Ruvkun, G., Thomas, J. H., and Swoboda, P. (2005). Analysis of *xbx* genes in *C. elegans*. Development *132*, 1923–1934.

Evans, J. E., Snow, J. J., Gunnarson, A. L., Ou, G., Stahlberg, H., McDonald, K. L., and Scholey, J. M. (2006). Functional modulation of IFT-kinesins extends the sensory repertoire of ciliated neurons in *C. elegans*. J. Cell Biol. *172*, 663–669.

Fan, Y., *et al*. (2004). Mutations in a member of the Ras superfamily of small GTP-binding proteins causes Bardet-Biedl syndrome. Nat. Genet. *36*, 989–993.

Fujiwara, M., Ishihara, T., and Katsura, I. (1999). A novel WD40 protein, CHE-2, acts cell-autonomously in the formation of *C. elegans* sensory cilia. Development *126*, 4839–4848.

Gross, C., De Baere, E., Lo, A., Chang, W., and Messiaen, L. (2001). Cloning and characterization of human *WDR10*, a novel gene located at 3q21 encoding a WD-repeat protein that is highly expressed in pituitary and testis. DNA Cell Biol. *20*, 41–52.

Haycraft, C. J., Banizs, B., Aydin-Son, Y., Zhang, Q., Michaud, E. J., and Yoder, B. K. (2005). Gli2 and Gli3 localize to cilia and require the intraflagellar transport protein polaris for processing and function. PLoS Genet. *1*, 480–488.

Haycraft, C. J., Schafer, J. C., Zhang, Q., Taulman, P. D., and Yoder, B. K. (2003). Identification of CHE-13, a novel intraflagellar transport protein required for cilia formation. Exp. Cell Res. *284*, 251–263.

Haycraft, C. J., Swoboda, P., Taulman, P. D., Thomas, J. H., and Yoder, B. K. (2001). The *C. elegans* homolog of the murine cystic kidney disease gene *Tg737* functions in a ciliogenic pathway and is disrupted in *osm-5* mutant worms. Development *128*, 1493–1505.

Howard, R. W., and Maurer, R. A. (2000). Identification of a conserved protein that interacts with specific LIM homeodomain transcription factors. J. Biol. Chem. *275*, 13336–13342.

Jekely, G., and Arendt, D. (2006). Evolution of intraflagellar transport from coated vesicles and autogenous origin of the eukaryotic cilium. BioEssays *28*, 191–198.

Kozminski, K. G., Johnson, K. A., Forscher, P., and Rosenbaum, J. L. (1993). A motility in the eukaryotic flagellum unrelated to flagellar beating. Proc. Natl. Acad. Sci. USA *90*, 5519–5523.

Kozminski, K. G., Beech, P. L., and Rosenbaum, J. L. (1995). The *Chlamydomonas* kinesin-like protein FLA10 is involved in motility associated with the flagellar membrane. J. Cell Biol. *131*, 1517–1527.

Lawrence, C. J., *et al*. (2004). A standardized kinesin nomenclature. J. Cell Biol. *167*, 19–22.

Li, D., and Roberts, R. (2001). WD-repeat proteins: structure characteristics, biological function, and their involvement in human diseases. Cell. Mol. Life Sci. *58*, 2085–2097.

Lin, B., White, J. T., Utleg, A. G., Wang, S., Ferguson, C., True, L. D., Vessella, R., Hood, L., and Nelson, P. S. (2003). Isolation and characterization of human and mouse WDR19, a novel WD-repeat protein exhibiting androgen-regulated expression in prostate epithelium. Genomics *82*, 331–342.

Lucker, B. F., Behal, R. H., Qin, H., Siron, L. C., Taggart, W. D., Rosenbaum, J. L., and Cole, D. G. (2005). Characterization of the intraflagellar transport complex B core: direct interaction of the IFT81 and IFT74/72 subunits. J. Biol. Chem. *280*, 27688–27696.

Malone, E. A., and Thomas, J. H. (1994). A screen for nonconditional dauer-constitutive mutations in *Caenorhabditis elegans*. Genetics *136*, 879–886.

Mello, C. C., Kramer, J. M., Stinchcomb, D., and Ambros, V. (1991). Efficient gene transfer in *C. elegans*: extrachromosomal maintenance and integration of transforming sequences. EMBO J. *10*, 3959–3970.

Morris, R. L., and Scholey, J. M. (1997). Heterotrimeric kinesin-II is required for the assembly of motile 9+2 ciliary axonemes on sea urchin embryos. J. Cell Biol. *138*, 1009–1022.

Munoz, J. M., and Riddle, D. L. (2003). Positive selection of *Caenorhabditis elegans* mutants with increased stress resistance and longevity. Genetics *163*, 171–180.

Murayama, T., Toh, Y., Ohshima, Y., and Koga, M. (2005). The *dyf-3* gene encodes a novel protein required for sensory cilium formation in *Caenorhabditis elegans*. J. Mol. Biol. *346*, 677–687.

Orozco, J. T., Wedaman, K. P., Signor, D., Brown, H., Rose, L., and Scholey, J. M. (1999). Movement of motor and cargo along cilia. Nature *398*, 674.

Ou, G., Blacque, O. E., Snow, J. J., Leroux, M. R., and Scholey, J. M. (2005a). Functional coordination of intraflagellar transport motors. Nature *436*, 583–587.

Ou, G., Qin, H., Rosenbaum, J. L., and Scholey, J. M. (2005b). The PKD protein qilin undergoes intraflagellar transport. Curr. Biol. *15*, 410–411.

Pazour, G. J., Dickert, B. L., and Witman, G. B. (1999). The DHC1b (DHC2) isoform of cytoplasmic dynein is required for flagellar assembly. J. Cell Biol. *144*, 473–481.

Pazour, G. J., and Rosenbaum, J. L. (2002). Intraflagellar transport and cilia-dependent diseases. Trends Cell Biol. *12*, 551–555.

Pedersen, L. B., Geimer, S., and Rosenbaum, J. L. (2006). Dissecting the molecular mechanisms of intraflagellar transport in *Chlamydomonas*. Curr. Biol. *16*, 450–459.

Perkins, L. S., Hedgecock, E. M., Thomson, J. N., and Culloti, J. G. (1986). Mutant sensory cilia in the nematode *Caenorhabditis elegans*. Dev. Biol. *117*, 456–487.

Piperno, G., and Mead, K. (1997). Transport of a novel complex in the cytoplasmic matrix of *Chlamydomonas* flagella. Proc. Natl. Acad. Sci. USA *94*, 4457–4462.

Piperno, G., Siuda, E., Henderson, S., Segil, M., Vaananen, H., and Sassaroli, M. (1998). Distinct mutants of retrograde intraflagellar transport (IFT) share similar morphological and molecular defects. J. Cell Biol. *143*, 1591–1601.

Porter, M. E., Bower, R., Knott, J. A., Byrd, P., and Dentler, W. (1999). Cytoplasmic dynein heavy chain 1b is required for flagellar assembly in *Chlamydomonas*. Mol. Biol. Cell *10*, 693–712.

Qin, H., Rosenbaum, J. L., and Barr, M. M. (2001). An autosomal recessive polycystic kidney disease gene homolog is involved in intraflagellar transport in *C. elegans* ciliated sensory neurons. Curr. Biol. *11*, 457–461.

Rappoport, J. Z., Simon, S. M., and Benmerah, A. (2004). Understanding living clathrin-coated pits. Traffic *5*, 327–337.

Rosenbaum, J. L., and Witman, G. B. (2002). Intraflagellar transport. Nature Reviews: Mol. Cell. Biol. *3*, 813–825.

Schafer, J. C., Haycraft, C. J., Thomas, J. H., Yoder, B. K., and Swoboda, P. (2003). XBX-1 encodes a dynein light intermediate chain required for retrograde intraflagellar transport and cilia assembly in *Caenorhabditis elegans*. Mol. Biol. Cell *14*, 2057–2070.

Scholey, J. (2003). Intraflagellar transport. Annu. Rev. Cell Dev. Biol. *19*, 423–443.

Signor, D., Wedaman, K. P., Orozco, J. T., Dwyer, N. D., Bargmann, C. I., Rose, L. S., and Scholey, J. M. (1999b). Role of a class DHC1b dynein in retrograde transport of IFT motors and IFT raft particles along cilia, but not dendrites, in chemosensory neurons of living *Caenorhabditis elegans*. J. Cell Biol. *147*, 519–530.

Signor, D., Wedaman, K. P., Rose, L. S., and Scholey, J. M. (1999a). Two heteromeric kinesin complexes in chemosensory neurons and sensory cilia of *Caenorhabditis elegans*. Mol. Biol. Cell *10*, 345–360.

Smith, T. F., Gaitatzes, C., Saxena, K., and Neer, E. J. (1999). The WD repeat: a common architecture for diverse functions. Trends Biochem. Sci. *24*, 181–185.

Snow, J. J., Ou, G., Gunnarson, A. L., Walker, M.R.S., Zhou, H. M., Brust-Mascher, I., and Scholey, J. M. (2004). Two anterograde intraflagellar transport motors cooperate to build sensory cilia on *C. elegans* neurons. Nat. Cell Biol. *6*, 1109–1113.

Starich, T. A., Herman, K. R., Kari, C. K., Yeh, W., Schackwitz, W. S., Schuyler, M. W., Collet, J., Thomas, J. H., and Riddle, D. L. (1995). Mutations affecting the chemosensory neurons of *Caenorhabditis elegans*. Genetics *139*, 171–188.

Swoboda, P., Adler, H., and Thomas, J. H. (2000). The RFX-type transcription factor DAF-19 regulates sensory neuron cilium formation in *C. elegans*. Mol. Cell *5*, 411–421.

Tabish, M., Siddiqui, Z. K., Nishikawa, K., and Siddiqui, S. S. (1995). Exclusive expression of *C. elegans* osm-3 kinesin gene in chemosensory neurons open to the external environment. J. Mol. Biol. *247*, 377–389.

Taulman, P. D., Haycraft, C. J., Balkovetz, D. F., and Yoder, B. K. (2001). Polaris, a protein involved in left-right axis patterning, localizes to basal bodies and cilia. Mol. Biol. Cell *12*, 589–599.

Ward, S., Thomson, N., White, J. G., and Brenner, S. (1975). Electron microscopical reconstruction of the anterior sensory anatomy of the nematode *Caenorhabditis elegans*. J. Comp. Neurol. *160*, 313–337.

White, J. G., Southgate, E., Thomson, J. N., and Brenner, S. (1986). The structure of the nervous system of the nematode *Caenorhabditis elegans*. Philos. Trans. R. Soc. Lond. B. Biol. Sci. *314*, 1–340.